

Fig. 2: C-patterns. CXFYMZ represents the numbers of contacts  $X$ , fixed surfaces  $Y$ , and movable surfaces  $Z$ . In the notation CXFYMZ, it always holds that  $X=Y+Z$ .

TABLE I: Success rates of PT tasks for different placement environments [%]

		$N^C$ *a				
		1	2	3	4	5
$N^F$ *b	1	100	75	50	25	0
	2	-	100	83	67	43
	3	-	-	100	75	-

\*a Number of contact surfaces

\*b Number of fixed surfaces

sum  $f_1 + f_2$  of two objectives: accuracy  $f_1$  and efficiency  $f_2$ .

Table I shows PT success rates for each C-pattern (number of contacts  $N^C$  and fixed surfaces  $N^F$ ). We rank C-patterns by PT success rate in descending order and define each set as a policy pattern. There are 10 policy patterns from  $P_0$  (all PP) to  $P_9$  (all PT), as illustrated in Fig. 3. For the object arrangement operation, we identify the policy pattern that maximizes  $f_1 + f_2$  among the ten patterns.

3) *Brute-Force Search for Task Determination Policy*: To determine the PP and PT tasks, a multi-objective optimization problem is solved to find C-patterns and identify the policy pattern that maximizes  $f_1 + f_2$ .

$f_1$  is the normalized success rate of arranging target objects, and  $f_2$  is the normalized task completion time.  $f_1$  equals 1 if the object is at the target location, and 0 if it exceeds the predetermined distance between adjacent

	C1F1M0	C2F2M0	C3F3M0	C3F2M1	C2F1M1	C4F3M1	C4F2M2	C5F3M2	C3F1M2	C5F2M3	C4F1M3	C5F1M4
P0												
P1												
P2												
P3												
P4												
P5												
P6												
P7												
P8												
P9												

Fig. 3: Task assignment table for policy-contact patterns

objects from the target.  $f_2$  represents the maximum task completion time, with 1 indicating full execution using PP and 0 indicating full execution using PT.

### C. Self-supervised Learning of Tossing Motion

A policy for determining joint angle parameters for a two-fingered gripper executing a tossing motion is derived using self-supervised learning with the  $\epsilon$ -greedy method. This task determination policy is refined through brute-force search. Building on previous self-supervised learning for tossing motions in box packing, we redesign state and reward functions for object arrangement operation. In the proposed PT, after grasping the object according to its shape, the tossing motion begins at the set arm joint angle, with the object released as the gripper opens to the final width. Tossing motion learning considers grasping, releasing, and landing posture.

The state  $s$  is defined by four dimensions: horizontal grasp position, vertical grasp position, gripper angle at grasping, and gripper opening width at grasping. Action  $a$  is defined by the joint angles of the second, third, and fourth joints of the arm with six joints during the tossing motion. The neural network uses the four-dimensional state space as input, with an action space output of  $28 \times 22 \times 16 \times 21 \times 15 \times 18$  dimensions, and two 256-dimensional hidden layers.

Given the wide action space search range, optimal solutions require efficient learning. This is achieved by starting with a tossing motion learned from a reward considering collisions with surrounding objects in the placement area and the appropriate gripper opening width at release, used as prior knowledge.

Action selection during learning uses the  $\epsilon$ -greedy method, which chooses the action with the highest Q-value with probability  $1 - \epsilon$  and a random action with probability  $\epsilon$ , specifically selecting action  $\hat{a}$  such that Equation (1).

$$\hat{a} = \begin{cases} \arg \max_a Q(s, a), & \text{with probability } 1 - \epsilon \\ \text{a random action}, & \text{with probability } \epsilon \end{cases} \quad (1)$$

This method facilitates acquiring appropriate Q-values for various actions regardless of the initial Q-value.

We then design the immediate reward value for the tossing motion result, assigning a reward  $R_{tr}$  for the success or failure of the release,  $R_{lr}$  for the rotation angle of the landing position relative to the target, and  $R_{lp}$  for the landing position. The immediate reward value is the sum of all rewards, as in Equation (2), and is calculated as follows:

$$\mathbb{R} = R_{tr} + \alpha R_{lr} + \beta R_{lp}, \quad (2)$$

where  $\alpha$  and  $\beta$  are weighting coefficients. The assignment methods for rewards  $R_{tr}$ ,  $R_{lr}$ , and  $R_{lp}$  are detailed in Equation (3), Equation (4), and Equation (5).

Equation (3) provides positive and negative rewards for success or failure, determined empirically. Equation (4) assigns a reward of 1 when the object lands at the same angle as the target posture and 0 at the furthest posture, with rewards increasing quadratically as the rotation angle error decreases.

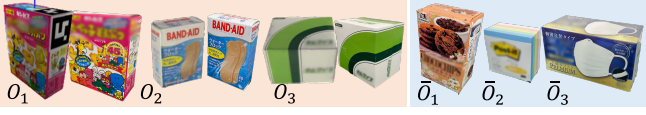


Fig. 4: Target objects.  $O_i$  ( $i \in \{1, 2, 3\}$ ) and  $\bar{O}_j$  ( $j \in \{1, 2, 3\}$ ) are the objects used (Trained) and not used (Unknown) in training

Equation (5) assigns a reward of 1 when the object lands within a non-collision range and 0 when it lands more than the width of a target object away, with rewards increasing linearly as the distance to the target position decreases.

$$R_{tr} = \begin{cases} 1 & (\text{release success}) \\ -10 & (\text{release failure}) \end{cases}, \quad (3)$$

$$R_{tr} = r_{roll} + r_{yaw},$$

$$r_{roll} = \begin{cases} 1/\bar{\theta}_{roll}^2(\theta_{roll} - \bar{\theta}_{roll})^2 & (\theta_{roll} \leq \bar{\theta}_{roll}) \\ 0 & (\theta_{roll} > \bar{\theta}_{roll}) \end{cases},$$

$$r_{yaw} = \begin{cases} 1/\bar{\theta}_{yaw}^2(\theta_{yaw} - \bar{\theta}_{yaw})^2 & (\theta_{yaw} \leq \bar{\theta}_{yaw}) \\ 0 & (\theta_{yaw} > \bar{\theta}_{yaw}) \end{cases}. \quad (4)$$

$$R_{lp} = r_x + r_y + r_z,$$

$$r_x = \begin{cases} 1 & (d_x \leq d_x^l) \\ -1/(d_x^h - d_x^l)d_x + d_x^h/(d_x^h - d_x^l) & (d_x^l < d_x \leq d_x^h) \\ 0 & (d_x > d_x^h) \end{cases},$$

$$r_y = \begin{cases} 1 & (d_y \leq d_y^l) \\ -1/(d_y^h - d_y^l)d_y + d_y^h/(d_y^h - d_y^l) & (d_y^l < d_y \leq d_y^h) \\ 0 & (d_y > d_y^h) \end{cases},$$

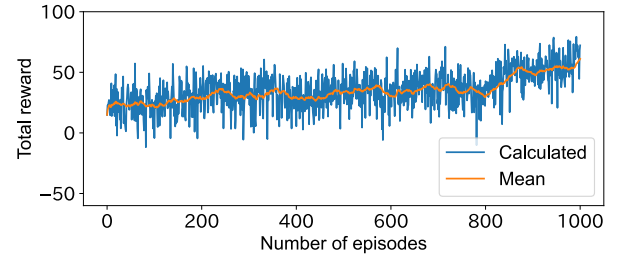
$$r_z = \begin{cases} 0 & (d_z \geq \bar{d}_z) \\ -1 & (d_z < \bar{d}_z) \end{cases}. \quad (5)$$

In this context, release success occurs when the target object is released from the gripper and tossed forward, while release failure happens if the object falls to the ground while still held by the gripper or before the arm reaches the release position.

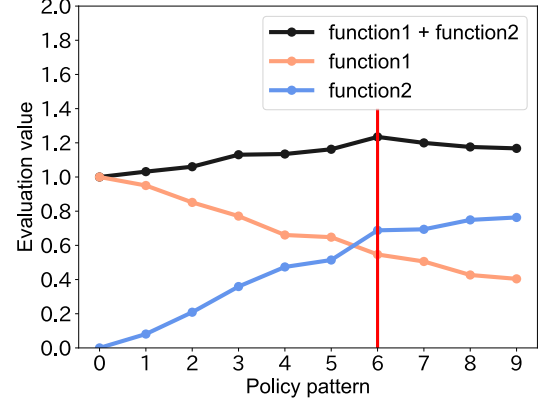
$\theta_{roll}$  and  $\theta_{yaw}$  are the roll and yaw angles from release to landing, and  $d_x$ ,  $d_y$ , and  $d_z$  indicate the distances between the landing and target positions in the  $x$ ,  $y$ , and  $z$  directions. These directions correspond to the  $XYZ$  axes shown in Fig. 1.  $\bar{\theta}_{roll}$  and  $\bar{\theta}_{yaw}$  are thresholds for rewarding errors in each rotation angle.  $d_x^l$  and  $d_y^l$  ensure a high reward area where the robot can land without hitting surrounding objects.  $d_x^h$  and  $d_y^h$  are based on the distance to the target object, and  $\bar{d}_z$  is set to the height of the target placement position.

### III. TRAINING RESULTS IN SIMULATIONS

As illustrated in Fig. 1, the experimental setup involved arranging placements and containers using a robotic arm (UR5e, Universal Robots) with a two-finger gripper (2F-140, Robotiq). Three types of rectangular shapes  $O_i$  ( $i \in \{1, 2, 3\}$ ) with different sizes were used as target objects, as shown in Fig. 4. The base width $\times$ depth $\times$ height [mm] of each



(a) Total reward values through 1000 learning episodes for  $O_1$



(b) Evaluation values for the policy patterns for  $O_1$

Fig. 5: Training results. In (a), the blue lines show the calculated values of the rewards and the orange lines show the mean values. In (b), the red line shows the determined policy pattern.

$O_i$  were  $116 \times 49 \times 135$ ,  $65 \times 30 \times 93$ , and  $133 \times 88 \times 120$ , respectively.

For DQN training, we used the following parameters: 1000 episodes, 30 steps per episode, initial  $\varepsilon$  of 0.95 decreasing to 0.05, a discount rate of 0.8, a learning rate of 0.001, and a batch size of 64. The brute-force search for task determination policies for PP and PT is computationally prohibitive. For example, arranging 20 target objects in a  $4 \times 5$  matrix yields  $2^{21} \times 5$  possible environments. Thus, we constrained the task to 48 environments, excluding similar configurations, to include all possible C-patterns.

We computed the mean value of  $f_1 + f_2$  for the object arrangement task for each policy pattern in Fig. 3 across these environments. Parameters  $\alpha$  and  $\beta$  in Equation (2) were set to one. Values for  $\bar{\theta}_{roll}$ ,  $\bar{\theta}_{yaw}$ ,  $d_x^l$ ,  $d_y^l$ ,  $d_x^h$ ,  $d_y^h$  and  $\bar{d}_z$  in Equation (3), Equation (4), and Equation (5) were 360, 180, 0.03, 0.03, 0.15, 0.06, and 0.3, respectively.

Fig. 5 (a) illustrates the immediate reward value transition during learning for  $O_1$ , with similar trends observed for  $O_2$  and  $O_3$ . The reward value increases with learning steps, validating the learning process.

Fig. 5 (b) shows the task determination policy results for  $O_1$ , with similar trends for  $O_2$  and  $O_3$ . Function1 represents accuracy  $f_1$ , and function2 denotes efficiency  $f_2$ ; their sum,  $f_1 + f_2$ , is highlighted in red at the maximum value. The general-purpose policy pattern for all target objects was determined as  $P_6$ , balancing accuracy and efficiency, which are trade-offs.

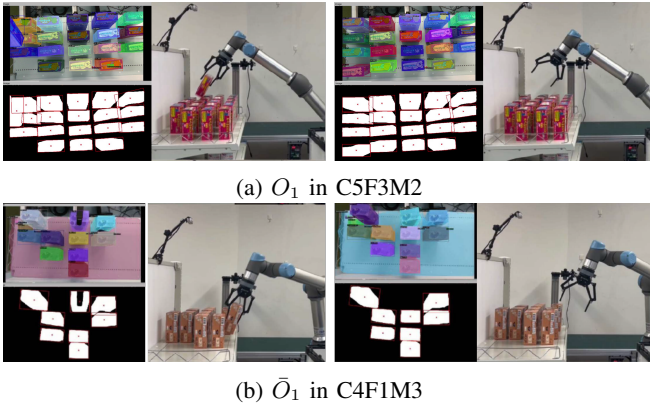


Fig. 6: Real-world tossing motions for the trained object in C5F3M2 (a)  $O_1$  and unknown object (b)  $\bar{O}_1$  in C4F1M3.

TABLE II: Success rates of real-world tossing motions [%]

C-pattern	Trained			Unknown		
	$O_1$	$O_2$	$O_3$	$\bar{O}_1$	$\bar{O}_2$	$\bar{O}_3$
C4F2M2	100	70	100	90	90	100
C5F3M2	100	60	90	90	70	80
C3F1M2	100	70	90	80	80	80

#### IV. REAL-WORLD FEASIBILITY

To check the feasibility in the real world, using the final estimated values of the joint angle parameters at the time of release obtained after learning as a reference, 10 trials were conducted for each of the three different C-patterns (C4F4M2, C5F3M2, and C3F1M2) for a rectangular shape in a real environment. In addition, we confirmed the effectiveness of the task determination policy with  $P_6$  by comparing the task success rate and task completion time with those of the other policies with  $P_3$  and  $P_9$ .

The objects used in the experiment included three types of objects  $O_i$  in Fig. 4 for training (Trained) and three types of objects  $\bar{O}_j$  for simulation (Unknown), totaling six types. The dimensions of the unknown objects were  $94 \times 59 \times 157$ ,  $75 \times 43 \times 75$ , and  $200 \times 100 \times 103$  (width  $\times$  depth  $\times$  height [mm]). For the tossing motion parameters of the unknown object, parameters for a trained object of similar shape (same category and smallest squared error for three sides) were used based on Chen *et al.* [7].

Fig. 6 (a) shows the tossing motion using a trained object  $O_1$  in C5F3M2, while Fig. 6 (b) displays the motion with an unknown object  $\bar{O}_1$  in C4F1M3. The robotic arm successfully released the object from the specified position and posture at the release joint angle output from the learned model, confirming that the object arrangement task is feasible using a tossing motion similar to projectile motion.

Table II shows the success rate of the tossing motion in 10 trials for each target object and environment. The success rate was higher for  $O_1$  and  $O_3$  compared to any unknown object, suggesting effective learning. For  $O_2$ , which was smaller and thinner, the tossing motion was more challenging. Although

the success rates for  $\bar{O}_1$ ,  $\bar{O}_2$ , and  $\bar{O}_3$  are lower than for trained objects  $O_1$  and  $O_3$ , they still maintain a minimum of 70%. The average success rate for the three types of unknown objects in three environments was high at 84%, demonstrating applicability to unknown objects by referencing similar shapes.

In addition, 10 trials were performed on the object placement task using PP and PT with the task determination policies of P3, P6, and P9. 12 objects were randomly placed in the workspace for the initial placement, and the task was to place the remaining 8 objects. As a result, the average success rate and task completion time for the 8 tasks of P3, P6, and P9 were 112 seconds for 88%, 80 seconds for 86%, and 76 seconds for 68%, respectively. The time required to repair failed tasks was not included in the task completion time. The results were comparable to those of the simulation, suggesting that the task determination policy of P6 can achieve balanced tasks in terms of success rate and task completion time in the real world.

#### V. CONCLUSIONS

Efficient robot operation in object arrangement is essential. This study introduces pick-and-toss (PT) to replace pick-and-place (PP), extending the robot's range and task efficiency. PT enhances efficiency, but environmental factors affect tossing success. Cluttered areas with many movable surfaces require caution to avoid collisions, whereas fixed surfaces like walls simplify the task. This study aims for accurate and efficient object arrangement by determining PP and PT tasks, considering placement environment difficulty. We proposed a method to simultaneously learn tossing motion through self-supervised learning and establish a task determination policy via brute-force search, proving effective in simulations and real-world tests.

Future work will focus on recognizing the grasping state affecting tossing motion and developing a self-supervised learning approach from limited real-world samples. With only 12 C-patterns currently available, we plan to create an open-ended model for PP and PT policy determination for additional C-patterns.

#### REFERENCES

- [1] T. Senoo, A. Namiki, and M. Ishikawa, "High-speed throwing motion based on kinetic chain approach," in *Proc. IEEE/RSJ Int. Conf. Intell. Rob. Syst.*, 2008, pp. 3206–3211.
- [2] H. Miyashita, T. Yamawaki, and M. Yashima, "Parts assembly by throwing manipulation with a one-joint arm," in *Proc. IEEE/RSJ Int. Conf. Intell. Rob. Syst.*, 2010, pp. 43–48.
- [3] S. Kajikawa and A. Knoll, "Analysis and modeling of hand-ball contact force during tossing motion," in *Proc. IEEE Int. Conf. Syst. Man. Cybern.*, 2014, pp. 51–56.
- [4] A. Takahashi, M. Sato, and A. Namiki, "Dynamic compensation in throwing motion with high-speed robot hand-arm," in *Proc. IEEE Int. Conf. Robot. Autom.*, 2021, pp. 6287–6292.
- [5] X. Zhou, R. Girdhar, A. Joulin, P. Krährenbühl, and I. Misra, "Detecting twenty-thousand classes using image-level supervision," in *Proc. Eur. Conf. Comput. Vis.*, 2022, pp. 350–368.
- [6] T. Yoshikawa, Y. Yokokohji, and Y. Yu, "Assembly planning operation strategies based on the degree of constraint," in *Proc. IEEE/RSJ Int. Conf. Intell. Rob. Syst.*, 1991, pp. 682–687.
- [7] H. Chen, T. Kiyokawa, W. Wan, and K. Harada, "Category-association based similarity matching for novel object pick-and-place task," *IEEE Robot. Autom. Lett.*, vol. 7, no. 2, pp. 2961–2968, 2022.